Inorganic Chemistry

Article

pubs.acs.org/IC

Terpyridine-Based Heteroditopic Ligand for $Ru^{II}Ln_3^{III}$ Metallostar Architectures (Ln = Gd, Eu, Nd, Yb) with MRI/Optical or Dual-Optical Responses

Alexandre Boulay,[†,‡] Céline Deraeve,[†,‡,#] Luce Vander Elst,[*,§,∥] Nadine Leygue,[†,‡] Olivier Maury,[⊥] Sophie Laurent,[§,∥] Robert N. Muller,[§,∥] Béatrice Mestre-Voegtlé,[*,†,‡] and Claude Picard[*,†,‡]

[†]CNRS, Laboratoire de Synthèse et Physico-Chimie de Molécules d'Intérêt Biologique, SPCMIB, UMR-5068, 118 Route de Narbonne, F-31062 Toulouse cedex 9, France

[‡]Université de Toulouse, UPS, Laboratoire de Synthèse et Physico-Chimie de Molécules d'Intérêt Biologique, SPCMIB, 118 route de Narbonne, F-31062 Toulouse cedex 9, France

[§]NMR and Molecular Imaging Laboratory, Department of General, Organic and Biomedical Chemistry, University of Mons, 23 Place du Parc, B-7000 Mons, Belgium

[∥]Center for Microscopy and Molecular Imaging (CMMI), Rue Adrienne Bolland, 8, B-6041 Gosselies, Belgium

[⊥]Université de Lyon 1, Laboratoire de Chimie de l'ENS Lyon, CNRS UMR 5182, 46 allée d'Italie, 69364 Lyon, France

Supporting Information

ABSTRACT: A new ditopic ligand (L) based on a 2,2′:5′,4″-terpyridine unit substituted in the 2″,6″ positions with iminodiacetate arms has been designed and synthesized for the construction of $Ru^{II}L_3Ln_3^{III}$ supramolecular architectures. The two components of this system, a 2,2′-bipyridine unit for Ru^{II} coordination and a pyridine-bis(iminodiacetate) core for Ln^{III} coordination, are tightly connected via a covalent $C_{arom}(py)-C_{arom}(py)$ bond. The paramagnetic and photophysical properties of the corresponding tetrametallic $Ru^{II}L_3Gd_3^{III}$ complex have been evaluated, highlighting the potential of this metallostar structure to act as a bimodal MRI/optical imaging agent. Variable-temperature ^{17}O NMR and proton nuclear magnetic relaxation dispersion (NMRD) measurements showed that this complex exhibits (i) a remarkable relaxivity per metallostar molecule, particularly at clinical and high magnetic fields (r_1^{310K} = 51.0 and 36.0 mM^{-1} s^{-1} at 20 and 300 MHz, respectively) and (ii) a near-optimal residence lifetime of Gd^{III} coordinated water molecule (τ_M^{310K} = 77.5 ns). This is the result of the presence of two inner-sphere water molecules in the Gd^{III} components of the metallostar and a slow tumbling rate of the molecule (τ_R^{310K} = 252 ps). Upon excitation in the visible domain (λ_{exc} = 472 nm), the Ru^{II} component of the complex exhibits a bright-red luminescence centered at 660 nm with a quantum yield of 2.6% in aqueous solutions at pH 7.4. Moreover, this $Ru^{II}L_3Gd_3^{III}$ assembly is also characterized by a high kinetic inertness in biological media (PBS and human serum solutions) and a high photostability (photobleaching). Finally, preliminary photophysical studies on RuL_3Nd_3 and RuL_3Yb_3 assemblies revealed that the Ru^{II} center acts as an effective sensitizer for Ln^{III}-based luminescence in the near-IR region. The Nd^{III} species was found to be the most effective at quenching the ^{3}MLCT luminescence of the Ru center.

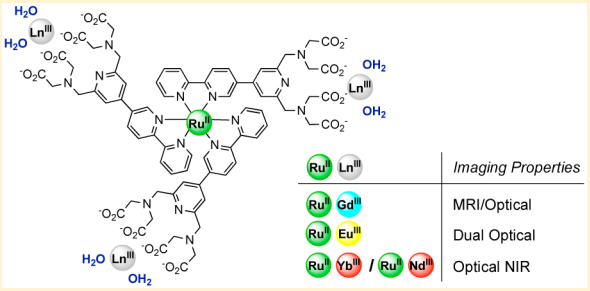

INTRODUCTION

In MRI domains, the use of gadolinium(III) contrast agents (CAs), commonly called T_1 or positive agents because they increase signal intensity, is well-established, and, currently, intensive research efforts are devoted to the design of more efficient Gd^{III}-based CAs.[1−4] In addition to their main applications in clinical diagnosis (∼30−40% MRI exams), they are also used in medical research and pharmacogical studies including in vitro and animal experiments.[5] The contrast efficiency, named relaxivity and symbolized by r_1, of Gd^{III}-based CAs currently in clinical use is relatively low ($r_1 \approx 4$ mM^{-1} s^{-1} at 20 MHz and 37 °C).[6] This implies the use of high concentrations (0.1 mM kg^{-1} total body weight) of these CAs, which does not limit them as bulk extracellular relaxation agents but becomes a severe limitation for their use as molecular MRI agents.[7] In this latter emerging MRI domain, a high relaxivity concentrated into a limited molecular volume is required for selected biological targets or specific cellular events.

The more straightforward and simplest procedure to allow a marked sensitivity enhancement deals with the use of architectures containing several Gd^{III} chelating units of sufficient relaxivity. Such systems concentrate several MRI probes in a small volume, but they may also enhance the

Received: September 30, 2014
Published: January 16, 2015

DOI: 10.1021/ic502342x
Inorg. Chem. 2015, 54, 1414−1425

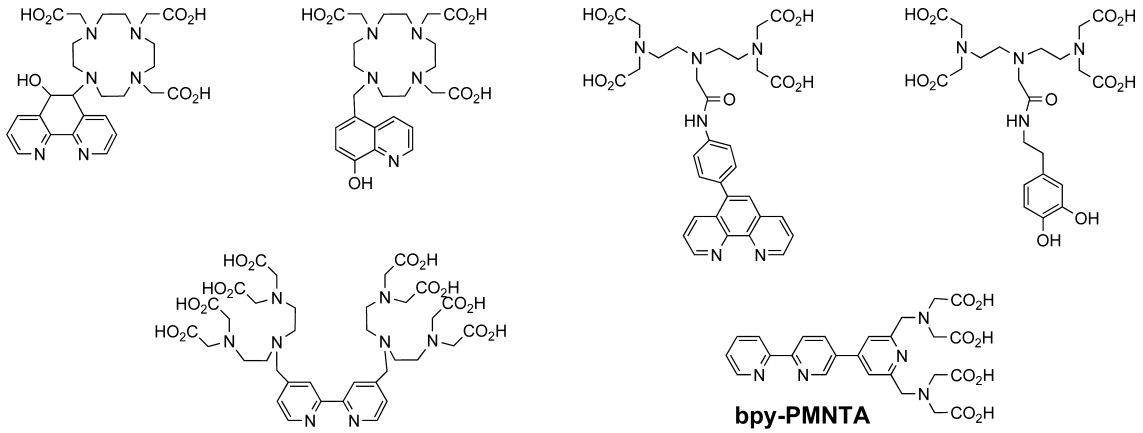

Figure 1. Examples of reported ligands structures in the construction of Gd_3M metallostars (M = Fe^{2+}, Ru^{2+}, Al^{3+}, Ti^{4+}) and bpy-PMNTA ligand structure.

intrinsic relaxivity properties of the Gd^{III} chelating unit. In such polymetallic architectures, the increase in relaxation per gadolinium is realized by slowing the rotational motion of the Gd^{III} chelating agent as a result of increased molecular weight of the system.[8]

In this direction, several works reported the covalent attachment of Gd^{III} chelates to macromolecules such as polyamino acids, polysaccharides, and dendrimers and to nanoparticles.[9−11] Another approach concerned midsize molecules and was based on the use of several Gd^{III} small chelates covalently attached to an organic platform (a single atom such as nitrogen or a small aromatic ring such as benzene)[12−14] or assembled in a rigid and compact space around a central *d*- or *p*-block metal ion (Fe^{II}, Ru^{II}, Al^{III}, Ti^{IV}).[15−27] As can be seen in Figure 1, these latter supramolecular heteropolymetallic compounds (also called metallostars) are based on polyfunctional ligands containing two different complexing moieties, each with structural features proper to the coordination mode of transition metal ion or lanthanide ion. For Fe^{II} or Ru^{II} chelation, 2,2′-bipyridine, phenanthroline, and 2,2′:6′,2″-terpyridine derivatives were employed, whereas bidentate ligands 8-hydroxyquinoline and catechol derivatives were utilized for Al^{III} and Ti^{IV} chelation, respectively. The complexing moiety for Gd^{III} binding was based on standard poly(aminocarboxylate) ligands such as DTPA (dietylenetriaminepentaacetate), DTTA (diethylenetriamine-*N*,*N*,*N*″,*N*″-tetraacetate), or DO3A (2,2′,2″-(1,4,7,10-tetraazacyclododecane-1,4,7-tryl)triacetate). At 20 MHz and 37 °C, the highest per Gd relaxivity enhancement ($r_1 \approx 25$ mM^{-1} s^{-1}) for the metallostars described in the literature was reported by Moriggi et al. for the Ru^{II} tris(adduct) of the $[Gd_2\{bpy(dtta)_2\}(H_2O)_4]^{2-}$ complex.[19] It is worth noting that pharmacokinetics and in vivo MRI feasibility studies of metallostars were also reported.[28,29] Additionally, it is important to note that most of the *d*- or *p*-metal ion centered heterometallic compounds offer photophysical properties of interest for their applications in the optical imaging field.[16,19,21−25] Yet, in recent years, growing attention has also been focused on the design of dual-modality probes possessing two signaling components for two imaging systems into a single structure.[30,31] In this direction, dual MRI−optical imaging contrast agents combine the high spatial resolution (micrometer), good temporal resolution (millisecond), and deep tissue penetration of MRI with the sensitivity (nano- to picomolar) of optical imaging probes.[32,33]

In this context, we designed a novel *d*−*f* metallostar contrast agent in which three gadolinium(III) complexes are assembled around a ruthenium(II) ion to a tetrametallic species. The ditopic ligand contains a PMNTA (abbreviated from [2,6-pyridinediylbis(methylene nitrilo)] tetraacetic acid) as the complexing unit for the Ln^{III} ion and a 2,2′-bipyridine core for the coordination of Ru^{II} (Figure 1). These two complexing units are tightly connected via a covalent $C_{arom}(py)-C_{arom}(py)$ bond, minimizing local flexibility arising from the linker that binds the two components and that might reduce the relaxivity gain achieved by the increased molecular size.[34] In Gd-PMNTA, the presence of two inner-sphere water molecules and an overall negative charge of the complex contribute to an efficient water exchange ($\tau_M^{310K} = 35.2$ ns) and a high relaxivity ($r_1 = 5.7$ mM^{-1} s^{-1} at 20 MHz and 310 K).[35] Moreover, the replacement of the metal-bound water molecules by bioactive bidentate anions such as L-lactate, citrate, carbonate, or bicarbonate has not been observed for Ln-PMMTA complexes.[36] The formation of such ternary complexes, which is common for DO3A-based heptatendate Ln^{III} complexes,[37] can be an important limitation to the MRI use of bishydrated Gd^{III} chelates. With respect to bisaqua Gd^{III} complexes, the stability constant of Gd-PMNTA (log $K = 18.6$) is comparable to those of Gd-DTTA derivatives (log $K = 18.2-18.6$) and about 2.5 orders of magnitude lower than that of Gd-DO3A (log $K = 21.1$).[38−40] We have chosen Ru^{2+} vs Fe^{2+} as the central *d*-transition metal ion for the formation of the supramolecular entity because it was reported that metallostars based on a $(Bpy)_3Fe^{2+}$ core do not have sufficient long-term stability in biological media.[18] Moreover, $(Bpy)_3Ru^{2+}$ can be utilized as an efficient luminescent probe. As a matter of fact, polypyridine complexes of ruthenium(II) display emission in the visible region with lifetimes in microsecond range that allows their use in time-resolved applications, large Stokes shift (>5000 cm^{-1}) that minimizes self-quenching, and high photostability that permits continuous monitoring of biological events by fluorescence spectroscopy and microscopy.[41,42] Thus, this heterometallic Gd_3Ru supramolecular assembly could serve as a potential MRI/optical bimodal agent, owing to it minimizing the differences in sensitivity of these two imaging modalities. Finally, considering such a Ru^{II} moiety, it can also act as a visible-light-excited antenna for sensitizing near-infrared (NIR) emitting Nd^{III} and Yb^{III} lanthanide ions. In this direction, several *d*−*f* and *d*−f_3 complexes based on these ions were reported as dual visible−NIR emitting probes.[43−45]

DOI: 10.1021/ic502342x
Inorg. Chem. 2015, 54, 1414−1425

Here, we report the synthesis and the paramagnetic and photophysical properties of this new tetrametallic Gd_3Ru supramolecular complex (Figure 2). The paramagnetic properties were investigated by oxygen-17 relaxometry and by proton relaxometry at various temperatures, magnetic fields, and media (pure water, phosphate buffer, and HSA-containing solutions). Luminescence properties (λ_{em}, Φ) of the Ru^{II} center and resistance against photobleaching of the Gd_3Ru assembly were investigated in aqueous solution at neutral pH. Stability tests on this metallostar were also realized in biological media (PBS and human serum). Finally, preliminary results related to the ability of NIR-emissive lanthanide ions (Nd^{III} and Yb^{III}) to act as energy acceptors from the Ru(II) core in the corresponding Nd_3Ru and Yb_3Ru assemblies are presented.

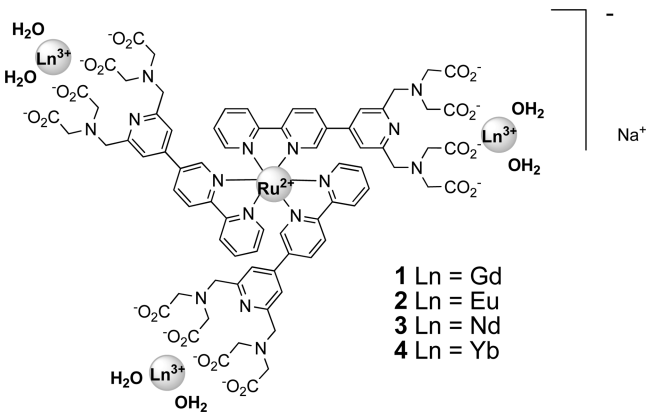

Figure 2. Ln_3Ru metallostars studied in this work.

RESULTS AND DISCUSSION

Ligand and Complexes Syntheses. Metallostar compounds studied in this work were obtained as depicted in Schemes 1 and 2. We used an uncommon approach, that is, by first preparing the *d*-block metal component and subsequently inserting Ln^{III} ions; the reverse order is usually reported for the construction of such *d*–*f* or *p*–*f* metallostar assemblies.[16−26]

The fully protected ligand **8** (Scheme 1) was synthesized by Pd(0)-catalyzed Stille cross-coupling protocols. In the first step, we took advantage of the differential reactivity of the two bromine substituents in 2,5-dibromopyridine toward oxidative addition in a Stille palladium-promoted coupling reaction. Indeed, 2-tributylstannylpyridine underwent Stille-type coupling with 2,5-dibromopyridine to give 5-bromo-2,2′-bipyridine in good yield (77%) by modification of the literature procedure.[46] In the subsequent step, our first attempts to obtain a trialkylstannylpyridine by lithiation and transmetalation by Me_3SnCl or nBu_3SnCl remained unsuccessful, and we turned to direct stannylation of **6** with hexaalkylditin.[47] With hexamethylditin and $Pd(PPh_3)_4$ as catalyst, the 5-stannylated product **6** was obtained in 89% isolated yield. The tetraester ditopic ligand **8** results from the reaction of trimethylstannyl derivative **6** and 4-bromo-2,6-bis[*N*,*N*-bis(*t*-butoxycarbonylmethyl)aminomethyl]pyridine **7**. This last compound was conveniently prepared in four steps from commercially available chelidamic acid as described by Takalo et al.[48] Finally, the Stille coupling reaction involving compounds **6** and **7** afforded the desired compound **8** in a good 71% yield after chromatographic purification.

Scheme 1. Synthesis of Fully Protected bpy-PMNTA Compound 8[a]

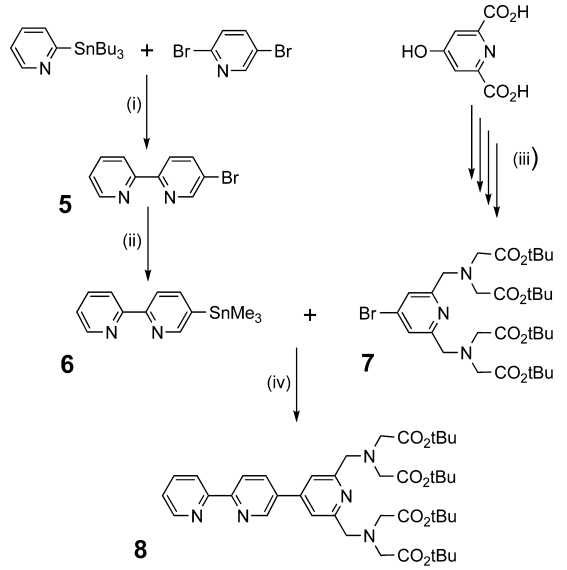

[a]Conditions: (i) $Pd(PPh_3)_4$, toluene, 48 h, reflux; (ii) $Me_3SnSnMe_3$, $Pd(PPh_3)_4$, dioxane, 20 h, reflux; (iii) see ref 48; (iv) CuBr, $Pd(PPh_3)_4$, toluene, 130 °C (microwave 260W), 90 min.

The ruthenium(II) complex **9** (Scheme 2) was obtained from the reaction of $Ru(DMSO)_4Cl_2$ with the bpy ligand **8** in refluxing ethanol followed by chromatography on silica gel and anion exchange with KPF_6. The red complex, isolated in 90% yield, was characterized by elemental analysis, MS, and ^1H, ^{13}C, and ^{19}F NMR spectroscopies. Its absorption spectrum in CH_3CN is typical for polypyridyl Ru^{II} complexes, with a band at 450 nm due to a spin-allowed $d \rightarrow \pi^*$ metal-to-ligand charge-transfer (^{1}MLCT) transition. In ESI^+-MS experiments, we observed several doubly or triply charged ions, e.g., $[M - 2PF_6]^{2+}$ at *m*/*z* 1172.1 or $[M - 2PF_6{+}H]^{3+}$ at *m*/*z* 781.7. It is worth noting that the fragmentation of this later triply charged ion is governed by the usual rupture of the *tert*-butyl ester bond, which leads to the observation of 10 successive losses of 18.7 Da (C_4H_8 fragment), confirming the presence of three ligands around the Ru ion. The ^1H NMR spectrum of **9** proved to be more complex than that of the free ligand due to the presence of *fac*- and *mer*-isomers. It is well-known that tris-unsymmetric diimine complexes of ruthenium(II) give rise to a mixture of *fac*-isomer (C_3 symmetry with the three ligands being chemically equivalent) and *mer*-isomer (C_1 symmetry with all three ligands in different chemical environments).[49−51] In the ^1H NMR spectrum of **9**, all of the aromatic protons are reported as multiplets, as the large number overlapping signals prevented detailed analysis. The methylene protons adjacent to the pyridine ring (3.83−3.89 ppm) and *tert*-butyl protons (1.33−1.38 ppm) each gave four sets of singlets. This seems to indicate the existence of a nearly statistical mixture of three *mer* to one *fac* and that this system does not rearrange to a preferred conformation.

Full deprotection of *tert*-butyl esters in **9** to reach the targeted complex **10** was achieved with a $TFA{-}CH_2Cl_2$ mixture at room temperature for 24 h. It is an easy and high-yield procedure and takes advantage of the very high stability of the $Ru(bpy)_3^{2+}$ core in acidic media.[52] The lanthanide complexes were easily obtained by treating an aqueous solution

DOI: 10.1021/ic502342x
Inorg. Chem. 2015, 54, 1414−1425

Scheme 2. Synthetic Route for Ln_3Ru Complexes 1−4[a]

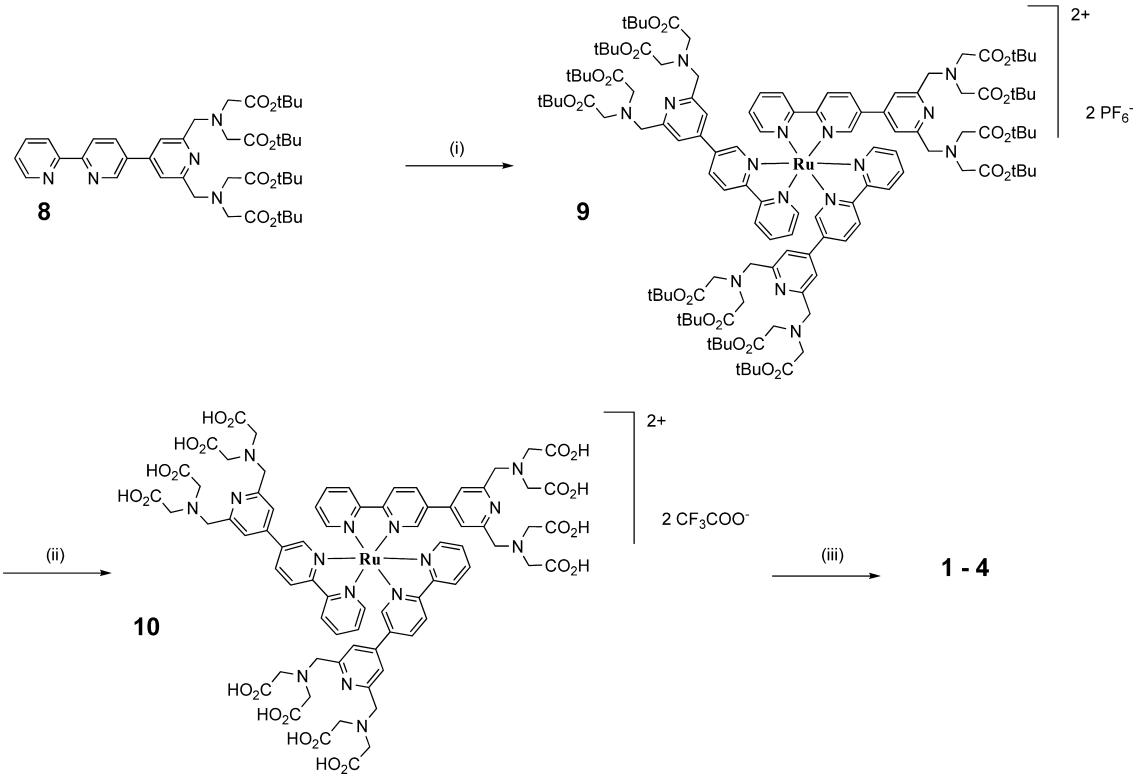

[a]Conditions: (i) (a) $Ru(DMSO)_4Cl_2$, EtOH, 48 h, reflux, (b) KPF_6, acetone; (ii) TFA, CH_2Cl_2, 24 h, rt; (iii) $LnCl_3{\cdot}6H_2O$, H_2O.

of Ru complex **10** with an excess of the lanthanide salt ($LnCl_3{\cdot}6H_2O$) to avoid any presence of mono- and di-lanthanide species. All complexes were purified by a Waters Sep-Pak column (C18), and the absence of free lanthanide ions was checked by the Arsenazo test.[53] The identity of the complexes was determined by mass spectrometric analyses and UV−visible absorption, and their purity was established by HPLC analyses. In MS spectra (ESI^-, ESI^+), all complexes exhibit peaks due to doubly charged species, with a good match between predicted and observed isotope patterns, thereby confirming the formation of the heterometallic compounds (Figure 3). Interestingly, the Ln^{III} (Ln = Gd, Eu, Nd, Yb) complexes showed similar retention times, suggesting that the Ln^{III} ions share the same coordination sphere in these metallostar architectures.

Relaxometric Studies. The ability of a Gd^{III} complex to act as a MRI contrast agent is generally described in terms of its relaxivity, that is, the longitudinal relaxation rate ($r_1 = 1/T_1$) increase of the water protons induced by 1 mM solution of the paramagnetic complex at a given temperature and magnetic field strength. At 20 MHz (a relevant field strength to compare MRI CAs), the proton relaxivity per metallostar molecule Gd_3Ru **1** in H_2O was measured to be 61.8 mM^{-1} s^{-1} at 298 K (51.0 mM^{-1} s^{-1} at 310 K). The corresponding r_1 value per Gd^{III} ion (20.6 and 17.0 mM^{-1} s^{-1} at 298 and 310 K, respectively) is significantly higher than that of parent complex Gd-PMNTA (5.7 mM^{-1} s^{-1} at 310 K) and those typical for bis-aqua Gd^{III} complexes of small size (relaxivities ranging from 6.0 to 10.2 mM^{-1} s^{-1} at 298 K).[54,55] The enhancement of relaxivity may be mainly attributed to the slower rotational correlation time (τ_R) due to the increase in molecular weight. Under these experimental conditions (20 MHz, 310 K), Gd_3Ru complex **1**

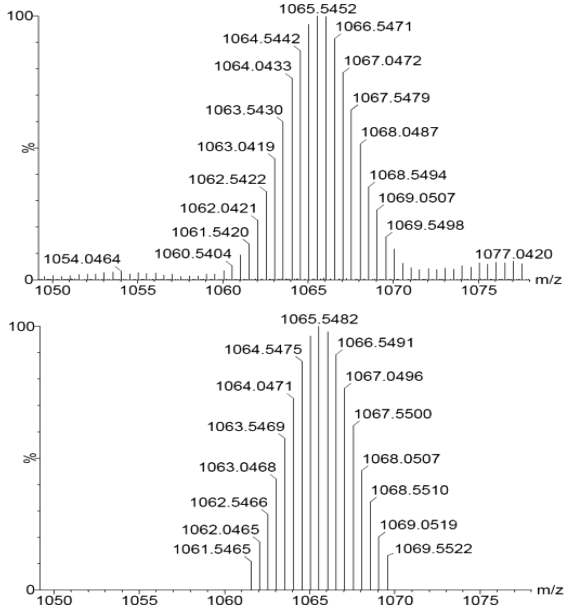

Figure 3. Observed (upper) and calculated (lower) isotope distributions for the doubly charged ion obtained by fragmentation of Gd_3Ru complex **1** (HRMS ESI^-).

showed also an increased proton relaxivity compared with that of Gd_3M metallostars (M = Fe, Ru, Al, Ti) of similar size reported in the literature (relaxivities r_1^{310K} ranging from 9.5 to 12.3 mM^{-1} s^{-1}).[15,21,22,24,25,29] The higher number of Gd^{III}-coordinated water molecules (q = 2 for our compound and q = 1 for these Gd_3M metallostars), resulting in higher relaxation, may account for this difference. Compared to the r_1 value of

DOI: 10.1021/ic502342x
Inorg. Chem. 2015, 54, 1414−1425

Gd_6Ru metallostar reported by Morrigi et al., that is $\{Ru[Gd_2bpy\text{-}DTTA_2(H_2O)_4]_3\}^{4-}$, the r_1 value per Gd^{III} ion of our compound is 1.5 times smaller, as expected from the ratio of their molecular weight (1.7).[19] Metallostar **1** exhibits high relaxivity, but it also has a relaxivity that is concentrated in a small molecular volume. In terms of efficiency per mass unit, a concept introduced by Livramento et al., metallostar **1** exhibits a density of relaxivity $\rho(r_1)$ of 27.6 and 22.8 $(g/L)^{-1}$ s^{-1} at 298 and 310 K, respectively.[56] These values compare favorably with those of Gd^{III}-based macromolecular MRI agents, such as Gd-chelate-loaded dendrimers or polysaccharides. As examples, a dendrimer loaded with 1157 Gd^{III} ions per molecule $[G_9\text{-}(GdEPTA)_{1157}]$ is characterized by a $\rho(r_1)$ value of 20.7 $(g/L)^{-1}$ s^{-1} at 20 MHz and 310 K, and a cyclodextrin loaded with ~7 Gd^{III} ions per molecule $[\beta\text{-CD-}(Gd\text{-}DOTA\ derivative)_{6.9}]$, by a $\rho(r_1)$ of 24.0 $(g/L)^{-1}$ s^{-1} at 20 MHz and 298 K.[34,57]

In order to determine the parameters that characterize water exchange (τ_M) and rotational dynamic (τ_R) for Gd_3Ru complex **1**, we performed a variable-temperature ^{17}O NMR study and proton relaxation rate measurements at different magnetic fields. The transverse ^{17}O relaxation rate was measured between 275 and 347 K at 500 MHz on an 8 mM solution of the complex. The ^1H nuclear magnetic relaxation dispersion profile (^1H NMRD) was determined at 310 K in the proton Larmor frequency range 10 kHz and 300 MHz, corresponding to magnetic field strengths varying between 2.35×10^{-4} and 7 T. These data are shown in Figures 4 and 5.

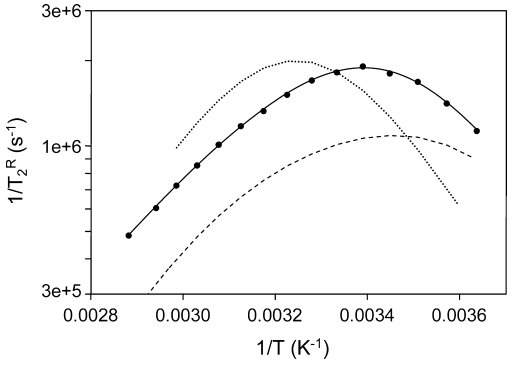

Figure 4. ^{17}O reduced transverse relaxation rate $(1/T_2^R)$ as a function of the reciprocal of the temperature for an aqueous solution of Gd_3Ru complex **1** at 11.75 MHz. The solid line corresponds to the theoretical fitting of the data points. The dotted and dashed lines correspond to the fitting of Gd-DTPA and Gd-PMNTA data, respectively.

The maximum of the curve of the evolution of the reduced transverse relaxation rate of ^{17}O with temperature corresponds to a temperature close to 295 K. This value is between those of Gd-DTPA (310 K) and Gd-PMNTA (290 K), qualitatively indicating an intermediate value of the residence time of coordinated H_2O molecules (Gd-DTPA, τ_M^{310K} = 143 ns; Gd-PMNTA, τ_M^{310K} = 35.2 ns). The theoretical treatment of the experimental data (Figure 4) was performed as previously described.[58,59] In the fitting, the number of inner-sphere water molecules was assumed to be q = 2, analogous to that of the parent Gd-PMNTA complex and in accordance with the data derived from the luminescence lifetime measurements on the corresponding Eu_3Ru metallostar assembly **2** (vide infra). From this fitting, the following parameters have been adjusted simultaneously: the residence time of the water molecules coordinated to the Gd^{III} ions (τ_M), the activation enthalpy

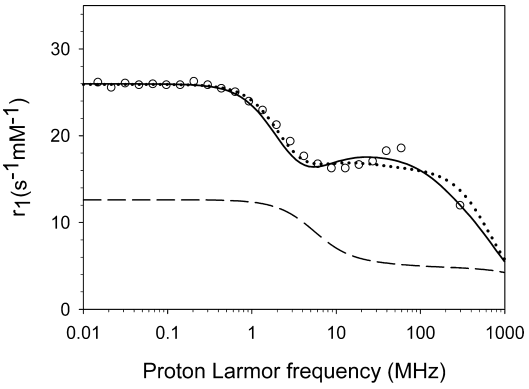

Figure 5. ^1H NMRD profile of Gd_3Ru complex **1** in water at 310 K (open circles) and Gd-PMNTA (dashed line) in water at 310 K. The solid and the dotted lines correspond to the Lipari–Szabo and classical theoretical fittings of the data points, respectively.

($\Delta H^{\ddagger}$) and entropy ($\Delta S^{\ddagger}$) for the water-exchange process, the hyperfine coupling constant between the oxygen-17 and the electronic spin of Gd^{III} ($A/\hbar$), the B-parameter, which is related to the mean-square of the zero-field-splitting energy ($B = 2.4\Delta^2$), and τ_v, the correlation time modulating the electronic relaxation of Gd^{III} (Table 1). The inclusion of Gd-PMNTA

Table 1. Parameters Obtained from the Theoretical Fittings of the ^{17}O Data of the Gd_3Ru Complex 1 in Water at 11.75 T

parameter	value
τ_M^{310K} [ns]	77.5 ± 6
$\Delta H^{\ddagger}$ [kJ mol^{-1}]	42.2 ± 0.1
$\Delta S^{\ddagger}$ [J mol^{-1} K^{-1}]	27.0 ± 0.3
$A/\hbar$ [10^6 rad s^{-1}]	−3.63 ± 0.03
B [10^{20} s^{-2}]	8.31 ± 0.3
τ_v^{298K} [ps]	18.5 ± 0.6
E_v [kJ mol^{-1}]	18.8 ± 2.6

units in a supramolecular structure has only a minor influence on the lability of the first-sphere water molecule. The calculated value of the water residence time at 310 K on the Gd_3Ru complex **1** (τ_M^{310K} = 77.5 ns) is about two times larger than that for Gd-PMNTA (τ_M^{310K} = 35.2 ns). This τ_M value compares favorably with those reported for *d*-Gd or *p*-Gd metallostars and does not limit the use of complex **1** for the design of magnetic tracers for molecular imaging. The large activation enthalpy, $\Delta H^{\ddagger}$, and the positive activation entropy, $\Delta S^{\ddagger}$, suggest a dissociative mechanism for the water exchange.[60] On the other hand, the assumption of bis-aqua Gd components in **1** was confirmed by the value of the $A/\hbar$ parameter, characteristic of q = 2 complexes of the Gd-PMNTA family.[61,62]

As can be seen from Figure 5, the ^1H NMRD profile of Gd-PMNTA displays the typical s-shape of low-molecular-weight and rapidly tumbling gadolinium(III) chelates: a plateau at low magnetic fields followed by a drop around 10 MHz leading to a lower level plateau in the high-field region (>60 MHz). Whatever the applied magnetic field, the relaxivity of Gd_3Ru complex **1** was higher and displayed a hump between 10 and 100 MHz with a maximum at 60 MHz (r_1^{310K} = 18.5 mM^{-1} s^{-1}), characteristic for slowly rotating molecules and assigned to the presence of a supramolecular structure. It is interesting to note that the relaxivity of Gd_3Ru complex **1** remains remarkably high at 300 MHz (11.9 mM^{-1} s^{-1} per Gd^{III} ion at 310 K). If

DOI: 10.1021/ic502342x
Inorg. Chem. 2015, 54, 1414−1425

most MRI machines work at 0.2−3 T for clinical exams, then higher fields (up to 9.4 T, 400 MHz) become commonly used for experimental animal studies.[63] A first theoretical adjustment of the NMRD profile was performed with the usual inner-sphere (IS) and outer-sphere (OS) contributions to the paramagnetic relaxation rate. The inner-sphere contribution is linked to water molecules bound to the Gd^{III} ion, whereas the outer-sphere contribution is referring to water molecules diffusing near the complex.[64] In the fitting procedure, parameters were fixed to common values in order to decrease the number of variables. The Gd^{III}−H distance (r_{GdH}) between the Gd^{III} ion and the proton nuclei of the bound water was fixed to 3.10 Å, the distance (d) of closest approach of an outer-sphere water proton to the Gd^{III} ion was set to 3.60 Å, and the relative diffusion coefficient (D), to 2.93×10^{-9} m^2 s^{-1}. The water residence time was fixed to the value determined by ^{17}O relaxometry. The parameters describing the rotational correlation time τ_R and the electronic relaxation times, τ_V and τ_{SO}, were optimized simultaneously and are reported in Table 2. The electronic relaxation time at zero field (τ_{SO}) of

Table 2. Relaxivities Values at 20 and 60 MHz (T = 310 K) and Parameters Obtained from the Theoretical Fittings of the ^{17}O Data and of the Proton NMRD Profile (T = 310 K) of the Gd_3Ru Complex 1 and Comparison with the Gd-PMNTA Complex

	Gd_3Ru complex **1**		Gd-PMNTA[a]
	IS + OS fit	Lipari−Szabo fit	IS + OS fit
τ_M [ns]	77.5[b]	70 ± 9.8	35.2 ± 3.0
τ_R [ps]	241 ± 3.0		56 ± 1
τ_{RG}[c] [ps]		788 ± 164	
τ_{RL}[d] [ps]		237 ± 14	
τ_{SO} [ps]	204 ± 3.2	225 ± 5.6	205 ± 15
τ_v [ps]	50.4 ± 3.4	45.3 ± 2.9	12.9 ± 3.8
S^2		0.12 ± 0.05	
r_1 [mM^{-1} s^{-1}][e]	17.0 (18.5)		5.7 (5.0)

[a]From ref 36. [b]Fixed to the value obtained for τ_M^{310K} by ^{17}O relaxometry. [c]Global rotational correlation time. [d]Local rotational correlation time. [e]At 20 (60) MHz.

metallostar **1** is similar to that of the Gd-PMNTA complex, and, as expected, the τ_R value of **1** (241 ps) is larger by a factor of 4.3. This longer rotational correlation time is associated with the larger dimension (molecular weight) of **1** and is mainly responsible for the 300% increase in r_1 of metallostar **1** as compared to that of the small contrast agent, Gd-PMNTA. In order to increase the agreement between the fitted and experimental data, a theoretical adjustment using the Lipari−Szabo model was applied. This approach has been previously used for the evaluation of NMR relaxation data for similar Gd systems.[13,18,24] The agreement between experimental and fitted data is slightly improved, but the results show a low coupling between global and local motions (S^2 = 0.12), whereas the other parameters are similar to those obtained with the classical inner-sphere and outer-sphere model.

We also evaluated the kinetic inertness of metallostar **1** by monitoring proton relaxivity at 20 MHz over a 58 h period in phosphate-buffered saline (PBS). The time dependence of the ratio $R_1^P(t)/R_1^P(0)$, where $R_1^P(t)$ is the relaxation rate at time t and $R_1^P(0)$ is the relaxation rate at time zero for complex **1** in 10 mM PBS (pH 7.4 and 310 K), is shown in Figure 6. We observed a slight decrease in R_1^P of ∼10% in the first 30 min (k_d

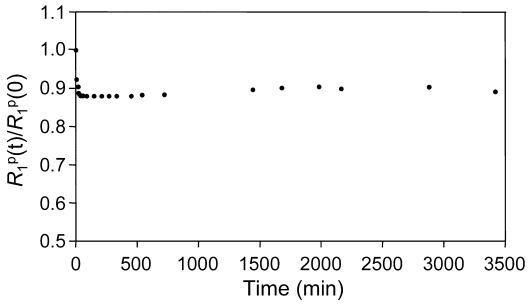

Figure 6. Kinetic stability of Gd_3Ru complex **1** in phosphate buffer (10 mM, pH 7.4) at 310 K. Evolution of the relative water proton paramagnetic relaxation rate $R_1^P(t)/R_1^P(0)$ at 20 MHz versus time.

= 0.128 min^{-1}), indicating a weak interaction of the complex with phosphate. This suggests that, under these experimental conditions, metallostar **1** is resistant toward dissociation of the $(bpy)_3Ru$ core and that the Gd^{III} inner-sphere water molecules are replaced by phosphate ions. In contrast, larger effects of phosphate on the relaxivity (∼70% decreasing) of the Gd_6Fe metallostar, that is, $\{Fe[Gd_2bpy\text{-}DTTA_2(H_2O)_4]_3\}^{4-}$, have been observed.[18] Finally, no significant binding of Gd_3Ru complex **1** with human serum albumin (HSA) was detected. In the presence of 4% HSA and at 310 K, the proton relaxation rates are slightly greater over the whole magnetic field range in the ^1H NMRD profile, and a r_1 relaxivity value of 18.7 mM^{-1} s^{-1} was observed at 20 MHz. Such a weak increase (∼10%) of the r_1 value does not indicate a significant interaction of the complex with HSA. As reported in the literature, a significant interaction between a Gd(III) complex and HSA is characterized by a greater than 60% increase in the relaxation rate.[65]

Photophysical Properties of Ru Complex 10 and Gd_3Ru Complex 1. The electronic absorption and emission properties of ruthenium complex **10** and Gd_3Ru metallostar **1** were recorded in nondegassed 50 mM Tris-buffered aqueous solutions (pH 7.4). The spectroscopic data of these complexes are summarized in Table 3, together with analogous data for the $[Ru(bpy)_3]^{2+}$ complex for comparison. Absorption spectra of solutions of **10** display an intense ligand-centered (LC) $\pi \rightarrow \pi^*$

Table 3. Photophysical Properties of Ru Complex 10 and Ln_3Ru Complexes 1−4 in Tris Buffer (50 mM, pH 7.4)

compd	λ_{abs} (nm) [ε (M^{-1} cm^{-1})]	λ_{em}^{298K} (nm)[a] [λ_{em}^{77K} (nm)][a]	Φ_{Ru}[b] (%)
$[Ru(bpy)_3]^{2+}$	285 [87 000]	625 [584, 630]	4.0[c]
	452 [14 500]		
10	299 [73 100]	656 [615, 668]	2.7
	468 [7100]		
1	300 [74 500]	660 [621, 671]	2.6
	472 [6900]		
2	300 [74 900]	616[d], 660	2.6
	472 [6900]		
3	300 [88 900]	660, 894, 1059	0.3
	472 [8300]		
4	300 [89 500]	660, 978	0.9
	472 [9500]		

[a]Excitation at 472 nm (^{1}MLCT absorption band). [b]Quantum yield of Ru^{II}-centered luminescence. [c]From ref 69. [d]Excitation at 300 nm (LC absorption band). The emission was recorded in time-resolved mode (delay time 50 μs).

DOI: 10.1021/ic502342x
Inorg. Chem. 2015, 54, 1414−1425

band at 299 nm (log ε = 4.86) as well as a broad and less intense band in the visible region around 468 nm (log ε = 3.85) attributed to the classical spin-allowed metal-to-ligand charge-transfer (^{1}MLCT) $d \rightarrow \pi^*$ transitions. Shoulders around 265 and 360 nm might be attributed to either LC or ^{1}MLCT transitions and to metal-centered (MC) $d \rightarrow d$ transitions, respectively.[66] When compared to $[Ru(bpy)_3]^{2+}$, the main difference is that the LC and ^{1}MLCT bands are significantly red-shifted (ca. 15 nm), owing to the extension of conjugation in the bpy-PMNTA moieties. Excitation into the ^{1}MLCT absorption band at 468 nm leads to a broad emission extending from 560 to 830 nm with a maximum at 656 nm at room temperature. Upon cooling the sample at 77 K, the emission maximum of the complex was blue-shifted (λ_{max} = 615 nm) compared to the emission at room temperature. With reference to related photophysical studies of $[Ru(bpy)_3]^{2+}$ and Ru^{II} polypyridine systems, the emission has been assigned to a ^{3}MLCT ($d\pi$(Ru) $\rightarrow$ π^*(bpy)) excited state.[67,68] When monitoring the emission at 656 nm, the excitation spectrum follows the absorption spectrum and presents two bands with maxima at ≈300 and 468 nm, showing that Ru(II) emission occurs from LC and ^{1}MLCT transitions. The quantum yield of the Ru^{II}-centered luminescence was determined by excitation into the ^{1}MLCT state, using $[Ru(bpy)_3]Cl_2$ (Φ = 4.0%)[69] on nondegassed water as a reference, and was found to be 2.7%. The coordination of the PMN moieties to Gd^{III} in metallostar **1** does not significantly influence the absorption and emission properties of the Ru^{II} center (Figure 7). Upon Gd^{III}

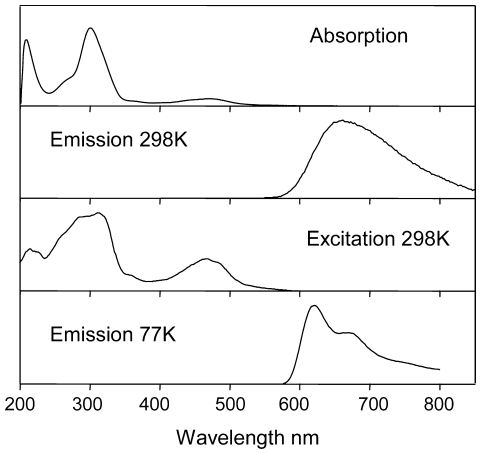

Figure 7. Normalized absorption, excitation, and luminescence spectra of 15 μM solutions of Gd_3Ru complex **1** in Tris buffer (50 mM, pH 7.4). A 298 K steady-state excitation spectrum was monitored at 660 nm. The 298 and 77 K steady-state emission spectra were monitored upon excitation at 472 nm.

complexation, the ^{1}MLCT absorption and ^{3}MLCT emission are slightly red-shifted (4 nm), and the emission quantum yield was found to be 2.6%. In Gd_3Ru complex **1**, the triplet energy level of the Ru^{II} center was calculated by reference to the lower wavelength emission edge (580 nm, 17 250 cm^{-1}) from the low-temperature phosphorescence spectrum. The lack of quenching of the Ru^{II} ^{3}MLCT state in complex **1** is expected since the Gd^{III} excited levels have energies (>31 000 cm^{-1}) much higher than those of MLCT states of Ru^{II} chromophore, preventing any Ru $\rightarrow$ Gd energy transfer process. The luminescence lifetime of these complexes could not be measured due to instrumental limitations.

No changes of absorption and emission spectra of Gd_3Ru complex **1** were observed in aerated solutions after several days at room temperature in Tris buffer (pH 7.4). Moreover, no decrease in the emission intensity of the ^{3}MLCT state and no changes in the shapes of emission and excitation spectra over a 58 h period were observed when metallostar **1** (25 μM) was incubated in PBS (10 mM) or a mixture of human serum/Tris buffer (2:1) at pH 7.4 and 37 °C (Figure 8a). Under these

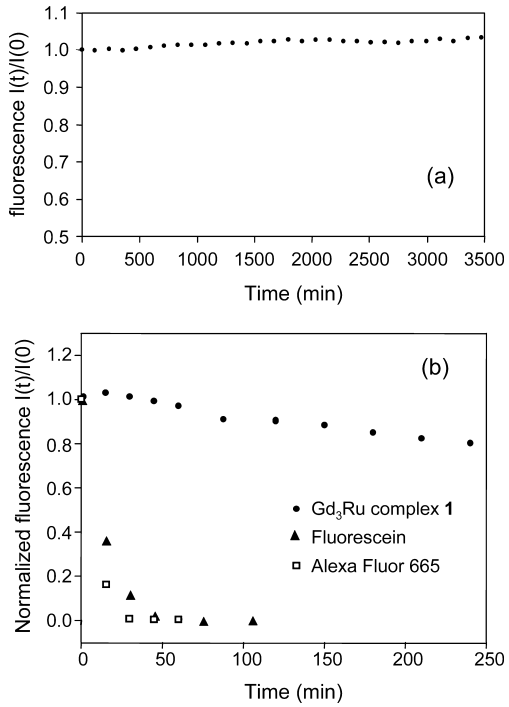

Figure 8. (a) Evolution of the relative total fluorescence intensity $I(t)/I(0)$ (λ_{exc} = 472 nm, λ_{em} = 660 nm) versus time in phosphate buffer (10 mM, pH 7.4) at 310 K of Gd_3Ru complex **1**. (b) Relative photobleaching profiles of Gd_3Ru complex **1**, fluorescein, or Alexa fluor 665 in Tris buffer (50 mM, pH 7.4) during continuous illumination with a xenon lamp excitation source. Fluorescence values were normalized to the initial intensity.

experimental conditions, these results confirm the robustness of the $(bpy)_3Ru$ core vs dissociation processes. We have also investigated the degree of photostability (photobleaching) of metallostar **1** and compared it to conventional fluorescent dyes, such as fluorescein and Alexa Fluor 665. The photostability was determined via measurements of the relative change in fluorescence intensity upon exposure to a white light from a xenon lamp in Tris buffer solutions at pH 7.4. Figure 8b clearly demonstrates that organic dyes showed a complete photofading after 1 h of constant illumination, whereas the luminescent emission of the metallostar retained 80% of its initial luminescence after 4 h of illumination. This demonstrates again that Ru^{II} complexes are less sensitive to photobleaching than are singlet-state fluorescent dyes. This good photostability is advantageous for its use in applications, allowing for a longer exposure time to excitation light and repeatability of experiments.

Photophysical Properties of Ln_3Ru Complexes (Ln = Eu, Nd, Yb). The absorption spectra of Ln^{III} complexes **2**–**4** are identical in terms of band shapes and positions to that of Gd_3Ru complex **1**, taken as a reference (Table 3). However, the

DOI: 10.1021/ic502342x
Inorg. Chem. 2015, 54, 1414–1425

relative intensity of the Ru^{II} ^{3}MLCT emission spectra of these three complexes differs greatly, as demonstrated in Figure 9a.

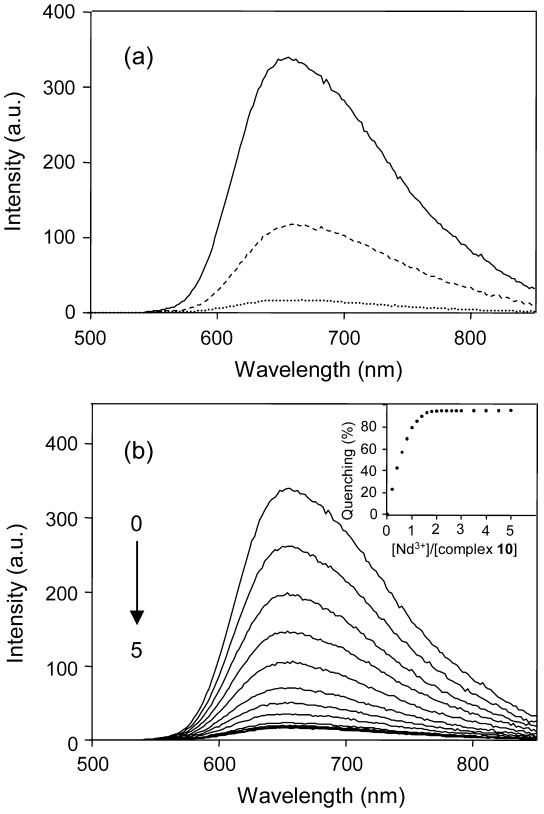

Figure 9. (a) Fluorescence emission spectra (λ_{exc} = 472 nm) of Gd_3Ru complex **1** (solid line), Nd_3Ru complex **3** (dotted line), and Yb_3Ru complex **4** (dashed line) showing the characteristic MLCT emission from the Ru^{II} center in Tris buffer solutions (50 mM, pH 7.4). (b) Evolution of the fluorescence spectrum of Ru complex **10** upon addition of $NdCl_3$ solutions in Tris buffer solutions (50 mM, pH 7.4).

As far as Eu_3Ru complex **2** is concerned, no quenching of the Ru^{II} ^{3}MLCT emission was observed under excitation into the ^{1}MLCT transition (λ_{exc} = 472 nm). At this excitation wavelength, no Eu^{III} emission was observed, neither in steady-state nor time-gated emission spectroscopies. On the contrary, upon excitation in the LC transition band (λ_{exc} = 300 nm), the typical emission pattern characteristic of the Eu^{III} ions ($^5D_0 \rightarrow {}^7F_J$, J = 0−4 transitions) can be clearly observed in the time-resolved luminescence mode with a 50 μs delay (Figure 10a). The hypersensitive $^5D_0 \rightarrow {}^7F_2$ and the sensitive $^5D_0 \rightarrow {}^7F_4$ transitions are dominant and account for ∼80% of the total emitted intensity. On the other hand, the excitation spectrum, obtained by recording the intensity of the $^5D_0 \rightarrow {}^7F_2$ transition at 616 nm as a function of excitation wavelength, resembles the absorption spectrum except for the ^{1}MLCT band at 472 nm. These results indicate that sensitization of the Eu^{III} luminescence at room temperature is possible only through the organic ligand and not by the MLCT states of Ru^{II} chromophore. This is in accordance with the highest energy ^{3}MLCT level of the Ru^{II} center, as determined at 77 K in the corresponding Gd_3Ru complex (17 250 cm^{-1}), which lies close to the Eu($^5D_0$) emitting level located at 17 300 cm^{-1}. With respect to the EuPMNTA complex, the crystal-field splitting of $^5D_0 \rightarrow {}^7F_J$ transitions of complex **2** is the same, and no changes in emission probabilities to different J levels are observed,

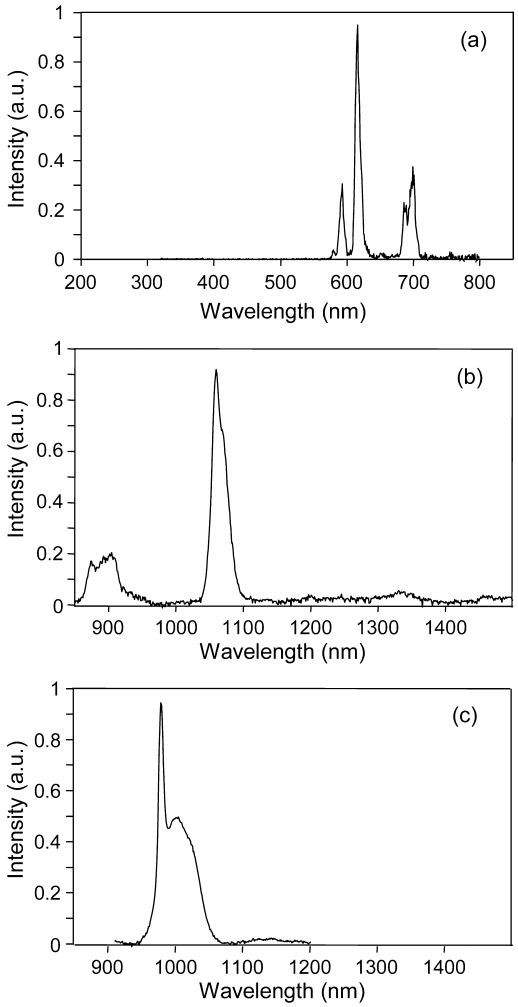

Figure 10. Visible emission at 298 K of Eu_3Ru complex **2** (a) under 300 nm (LC) excitation and recorded with a 50 μs delay and NIR emission spectra at 298 K of Nd_3Ru complex **3** (b) and Yb_3Ru complex **4** (c) under 472 nm (MLCT) excitation. Solutions are in Tris buffer (50 mM, pH 7.4).

indicating that the local coordination environment around Eu^{III} remains similar in these two complexes. The hydration state q of the europium component in Eu_3Ru complex **2** was evaluated by comparison of the luminescence lifetimes of the europium-centered emission in H_2O (τ_H) and D_2O (τ_D) solutions and by using the empirical equation proposed by Supkowski and Horrocks.[70] At 298 K, the lifetimes τ_H (0.270 ms) and τ_D (0.700 ms) point to the presence of two metal-bound water molecules per Eu^{III} ion (q = 2.18). These emission lifetimes are somewhat surprising since bis-hydrated Eu complexes usually have longer lifetime values. The $^5D_0$ lifetime in deuterated water increases up to 2 ms at 77 K, indicating that the Eu^{III} luminescence is quenched at room temperature by a temperature-dependent mechanism.

The emission spectra (λ_{exc} = 472 nm) of Nd_3Ru complex **3** and Yb_3Ru complex **4** showed that the emission intensity of the Ru^{II} center is quenched compared to that of the Gd_3Ru complex (Figure 9a), with a quenching more pronounced in the case of the Nd_3Ru complex. The emission intensity arising from the Ru^{II} ^{3}MLCT state is reduced by 90% (complex **3**) and 65% (complex **4**). This is indicative of effective energy migration between the Ru^{II} chromophore to the Nd^{III} and Yb^{III} moieties

DOI: 10.1021/ic502342x
Inorg. Chem. 2015, 54, 1414−1425

in these heterometallic structures. These results are corroborated by the luminescence intensity titration of Ru^{II} complex **10** with $NdCl_3$ and $YbCl_3$. In these experiments, the intensity of the ^{3}MLCT state emission decreases until a Ln^{III}/complex **10** concentration ratio of 1.8, and then a plateau is observed at higher concentration ratios (Figure 9b in the case of the titration with $NdCl_3$). The excitation of these complexes at 472 nm produces NIR emission that is characteristic of Nd^{III} and Yb^{III} ions (Figure 10b,c). Specifically, the Nd^{III} complex displayed emission within the 850−1400 nm range dominated by a broad band at 1059 nm ($^4F_{3/2} \rightarrow {}^4I_{11/2}$) with weak features at ca. 894 and 1330 nm, assigned to the $^4F_{3/2} \rightarrow {}^4I_{9/2}$ and $^4F_{3/2} \rightarrow {}^4I_{11/2}$ transitions, respectively. The steady-state emission spectrum of Yb_3Ru complex gave an emission within the 900−1100 nm range, assigned to the $^2F_{5/2} \rightarrow {}^2F_{7/2}$ transition, with a sharp band at 978 nm. For $RuYb_3$ and $RuNd_3$ structures based on a $Ru(Phen)_3$ core and Ln-cyclen-based ligands, Nonat et al. reported NIR emissions with quantum yields in the range 0.040−0.075%.[43] In our case, one can anticipate the quantum yields of complexes **3** and **4** to be rather lower, as their Yb^{III} and Nd^{III} components present two water molecules in their coordination spheres.

CONCLUSIONS

In this article, the design of new tetranuclear heterobimetallic complexes Ln_3Ru (Ln = Gd, Eu, Nd, Yb) is presented. These metallostar architectures were based on an original ditopic ligand with a bipyridine moiety and a PMNTA chelating unit that are closely connected. The Gd_3Ru assembly exhibits, at 310 K, a high r_1 relaxivity per Gd^{III} ion at clinical and high magnetic fields (r_1 = 17.0 and 11.9 mM^{-1} s^{-1} at 20 and 300 MHz, respectively). This complex is characterized by a fast water-exchange rate (τ_M^{310K} = 77.5 ns) and a slow tumbling rate ($\tau_R^{310K} \sim$ 240 ps). It also shows interesting photophysical properties, with excitation and emission in the visible domain (472/660 nm, respectively), and a fluorescence quantum yield of 2.6% in aqueous solutions at neutral pH. These luminescent and relaxometric properties are retained under biologically relevant conditions. This opens the way for the development of Gd_3Ru metallostar **1** or derivatives as bimodal contrast agents for MRI and optical imaging. Furthermore, preliminary photophysical data determined for Nd_3Ru and Yb_3Ru assemblies demonstrate the feasibility of a polypyridine-Ru center to act as a sensitizer for the NIR emission of Nd^{III} and Yb^{III} bis-hydrated complexes.

EXPERIMENTAL SECTION

Instruments. ^{1}H and ^{13}C spectra were recorded on Bruker Avance 300 and 500 MHz spectrometers; chemical shifts are given in ppm according to the solvent peak, and coupling constants (J) are given in Hertz (Hz). Multiplicities were recorded as s (singlet), d (doublet), t (triplet), q (quadruplet), and m (multiplet). Electrospray (ES) mass spectra were obtained on a Q TRAP Applied Biosystems spectrometer, and high-resolution mass spectra (HRMS), on a Xevo G2 QToF Waters spectrometer. Elemental analyses were carried out by the Service d'Analyse, Laboratoire de Chimie de Coordination (Toulouse). Absorption measurements were recorded with a Hewlett-Packard 8453 temperature-controlled spectrometer in a 10 mm quartz cuvette. Analytical HPLC was performed on a Waters Alliance 2695 system with a PDA 2996 detector using a reverse-phase column (Phenomenex Luna C8, 5 μM, 100 Å, 150 × 4.6 mm) with a flow rate of 1 mL/min. For systems A and B, solvents were H_2O containing 0.1% TFA (solvent A) and acetonitrile (solvent B). For system A, analyses were performed using the HPLC gradient system beginning with a solvent composition of 50% A/50% B and following a linear gradient up to 0% A/100% B from 0 to 18 min. For system B, the HPLC gradient system used begins with a solvent composition of 90% A/10% B and follows a linear gradient up to 10% A/90% B from 0 to 18 min. System C: solvents were 10 mM, pH 4, ammonium formate buffer (solvent A) and acetonitrile (solvent B); analyses were performed using the HPLC gradient system beginning with a solvent composition of 100% A and following a linear gradient up to 50% A/50% B from 0 to 18 min.

Photophysical Measurements. Fluorescence spectra in the visible region of the spectrum were obtained using LS-50B PerkinElmer and Cary Eclipse spectrofluorimeters equipped with a Xenon flash lamp source and a Hamamatsu R928 photomultiplier tube. The measurements were carried out at pH 7.4 in Tris buffer (50 mM), and all samples were prepared with an absorbance between 0.01 and 0.05 at the excitation wavelength in order to prevent the inner-filter effect. Phosphorescence spectra at 77 K were recorded with the LS-50B PerkinElmer spectrofluorimeter equipped with the low-temperature accessory no. L2250136. Spectra were corrected for both the excitation light source variation and the emission spectral response. The fluorescence quantum yields (uncertainty ±15%) were determined by using $[Ru(bpy)_3]^{2+}$ in aerated water as standard (Φ = 0.04)[69] and corrected for the refractive index of the solvent. The luminescence decay curves of the Eu^{III} complex were fitted by an equation of the form $I(t) = I(0)\exp(-t/\tau)$ by using a curve-fitting program. The number of metal-coordinated water molecules at 298 K was calculated using the following equation: $q_{H_2O}(Eu) = 1.11[(\tau_{H_2O})^{-1} - (\tau_{D_2O})^{-1} - 0.31]$.[70]

Fluorescence measurements in the NIR region were conducted on a Horiba-Jobin Yvon Fluorolog-3 spectrofluorimeter, equipped with a three slit double grating excitation and emission monochromator with dispersions of 2.1 nm/mm (1200 grooves/mm). The steady-state fluorescence was excited by unpolarized light from a 450 W xenon CW lamp and detected by a red-sensitive Hamamatsu R928 photomultiplier tube. Spectra were reference corrected for both the excitation source light intensity variation (lamp and grating) and the emission spectral response (detector and grating). Uncorrected near-infrared spectra were recorded using a liquid nitrogen cooled, solid indium/gallium/arsenic detector (850−1600 nm). An RG 830 filter was inserted in the emission pathway to suppress all visible light. The experimental data were treated using Origin software (normalization and baseline correction).

NMR Measurements. ^{17}O NMR measurements of solutions were performed at 11.75 T on 0.35 mL samples contained in 5 mm o.d. tubes on a Bruker Avance 500 MHz spectrometer. The temperature was regulated by air or nitrogen flow controlled by a Bruker BVT 3200 unit. Longitudinal proton relaxation rates were measured at 0.47 T and 310 K on a Minispec mq-20 (Bruker, Karlsruhe, Germany) instrument with a standard inversion−recovery sequence. Proton nuclear magnetic relaxation dispersion (NMRD) profile was recorded on a Stelar relaxometer (Mede, Italy) working between 0.24 mT and 1 T. The additional relaxation rates at 0.47, 1.41, and 7.05 T were measured on mq-20 and md-60 minispec systems and on a AMX300 spectrometer (all from Bruker, Karlsruhe, Germany). Fitting of the ^{1}H NMRD was performed with data-processing software using different theoretical models describing the nuclear relaxation phenomena observed (Minuit, CERN Library).[71,72] The exact Gd^{3+} concentration was determined by proton relaxivity measurements at 0.47 T and 37 °C after complete hydrolysis in concentrated HNO_3.

Synthesis of 5-Bromo-2,2′-bipyridine (5). To a solution of 2,5-dibromopyridine (0.712 g, 3.01 mmol) in anhydrous toluene (8 mL) was added 2-tributylstannylpyridine (0.88 mL, 2.72 mmol), and the reaction mixture was degassed by bubbling argon through the solution for 1 h. $Pd(PPh_3)_4$ (0.031 g, 0.027 mmol) was then added, and the mixture was refluxed for 48 h. After cooling to room temperature, the solids were removed by filtration, and the filtrate was concentrated in vacuo. Aqueous HCl (1 M) was added to the crude product, and the aqueous layer was washed with dichloromethane, neutralized with solid $NaHCO_3$, and extracted with dichloromethane. The resulting

DOI: 10.1021/ic502342x
Inorg. Chem. 2015, 54, 1414−1425

organic phase was dried ($MgSO_4$) and evaporated in vacuo. Purification by chromatography (alumina, petroleum ether/EtOAc 98:2) provided **5** as a white solid (0.489 g, 77%). mp 73−74 °C (lit.[46] 73 °C). TLC (alumina, petroleum ether/EtOAc 98:2) R_f = 0.58. ^{1}H and ^{13}C NMR data are in accordance with those in ref 46.

Synthesis of 5-Trimethylstannyl-2,2′-bipyridine (6). A solution of 5-bromo-2,2′-bipyridine **5** (200 mg, 0.851 mmol) in anhydrous dioxane (16 mL) was degassed by argon bubbling for 30 min. Hexamethylditin (554 mg, 1.69 mmol) in degassed dioxane (4 mL) and $Pd(PPh_3)_4$ (98 mg, 0.085 mmol) were then added, and the mixture was refluxed for 20 h. After cooling to room temperature, the solvents were evaporated, and the crude product was purified by chromatography (alumina, petroleum ether/EtOAc 100:0 to 98:2) to provide **6** as a colorless oil (242 mg, 89%). TLC (alumina, petroleum ether/EtOAc 98:2) R_f = 0.48. ^{1}H NMR (300 MHz, $CDCl_3$) δ 8.70 (s, 1H), 8.68 (dd, J = 0.9, 4.8 Hz, 1H), 8.40 (d, J = 7.8 Hz, 1H), 8.33 (dd, J = 0.9, 7.8 Hz, 1H), 7.92 (dd, J = 1.5, 7.8 Hz, 1H), 7.81 (td, J = 1.8, 7.5 Hz, 1H), 7.30 (ddd, J = 1.5, 4.8, 7.5 Hz, 1H), 0.37 (s, J Sn−H = 54/56 Hz, 9H). ^{13}C NMR (75 MHz, $CDCl_3$) δ 156.5 (Cq), 155.7 (Cq), 155.0 (CH), 149.2 (CH), 144.5 (CH), 137.7 (Cq), 136.9 (CH), 123.7 (CH), 121.0 (CH), 120.9 (CH), −9.5 (CH_3, J Sn−C = 341/357 Hz). MS (ESI$^+$) m/z (%) = 317/319/321 (12) $[M + H]^+$, 339/341/343 (100) $[M + Na]^+$. HRMS (ESI$^+$) calcd for $C_{13}H_{16}N_2NaSn$ $[M + Na]^+$, m/z 343.0233; found, m/z 343.0219.

Synthesis of 4-(2,2′-Bipyridine-5-yl)-2,6-bis[*N,N*-bis(*t*-butoxycarbonylmethyl)aminomethyl]pyridine (8). To a solution of compounds **7** (176 mg, 0.262 mmol) and **6** (100 mg, 0.313 mmol) in anhydrous toluene (5 mL) were added copper(I) bromide (6 mg, 0.042 mmol) and $Pd(PPh_3)_4$ (60 mg, 0.052 mmol). The solution was degassed in vacuo and transferred under argon to a microwave reactor. The mixture was heated at 130 °C under microwave irradiation (300 W) for 90 min. After cooling to room temperature, the solvents were evaporated, and the crude product was purified by chromatography (alumina, petroleum ether/EtOAc 90:10 to 80:20) to provide **8** as colorless oil (140 mg, 71%). TLC (alumina, petroleum ether/EtOAc 85:15) R_f = 0.30. ^{1}H NMR (300 MHz, $CDCl_3$) δ 9.03 (d, J = 1.8 Hz, 1H), 8.70 (dd, J = 0.9, 4.8 Hz, 1H), 8.49 (d, J = 8.4 Hz, 1H), 8.47 (d, J = 8.1 Hz, 1H), 8.15 (dd, J = 2.4, 8.4 Hz, 1H), 7.86 (s, 2H), 7.83 (dd, J = 1.8, 7.8 Hz, 1H), 7.33 (ddd, J = 0.9, 4.8, 7.5, 1H), 4.11 (s, 4H), 3.52 (s, 8H), 1.45 (s, 36H). ^{13}C NMR (75 MHz, $CDCl_3$) δ 170.6 (Cq), 159.9 (Cq), 156.2 (Cq), 155.7 (Cq), 149.3 (CH), 147.8 (CH), 146.1 (Cq), 137.0 (CH), 135.5 (CH), 134.2 (Cq), 123.9 (CH), 121.4 (CH), 120.9 (CH), 118.7 (CH), 81.1 (Cq), 59.9 (CH_2), 55.9 (CH_2), 28.2 (CH_3). MS (ESI$^+$) m/z (%) = 748.4 (37) $[M + H]^+$, 770.3 (100) $[M + Na]^+$, 786.4 (6) $[M + K]^+$. HRMS (ESI$^+$) calcd for $C_{41}H_{58}N_5O_8$ $[M + H]^+$, m/z 748.4285; found, m/z 748.4261.

Synthesis of Ruthenium(II) Complex [9] $(PF_6)_2$. To a stirring solution of **8** (50 mg, 66.9 μmol) in EtOH (10 mL) was added $Ru(DMSO)_4Cl_2$[73] (11 mg, 22.3 μmol), and the mixture was degassed by bubbling argon for 30 min. The solution was then allowed to reflux for 48 h. After cooling to room temperature, the solvents were removed in vacuo, and the crude product was purified by chromatography (silica gel, acetonitrile/H_2O/KNO_3 sat 100:7:1). The resulting product was dissolved in a minimum amount of acetone, precipitated with saturated aqueous solution of KPF_6, and filtered to provide **9** as a red powder (53 mg, 90%). HPLC (system A): t_R = 13.24 min. ^{1}H NMR (500 MHz, CD_3CN) δ 8.74−8.58 (m,6H), 8.38−8.33 (m, 3H), 8.15−8.10 (m, 3H), 7.93−7.86 (m, 6H), 7.49−7.37 (m, 9H), 3.89, 3.88, 3.84, and 3.83 (4 s, 12H), 3.42−3.26 (m, 24H), 1.38, 1.36, 1.35, and 1.33 (4 s, 108 H). ^{13}C NMR (125 MHz, CD_3CN) δ 171.5 and 171.4 (Cq), 161.0−160.7 (4 signals, Cq), 158.1−157.3 (3 signals, Cq), 153.2−152.9 (4 signals, CH), 150.4−150.2 (4 signals, CH), 144.2−144.0 (3 signals, Cq), 139.1 and 139.0 (CH), 136.9−136.8 (3 signals, CH), 129.1−128.7 (3 signals, CH),126.0−125.5 (5 signals, CH), 120.1−119.7 (3 signals, CH), 81.8 (Cq), 60.7−60.5 (3 signals, CH_2), 56.85−56.7 (3 signals, CH_2), 28.2 (CH_3). ^{19}F NMR (300 MHz, CD_3CN) δ −72.87 ($^1J_{PF}$ = 749 Hz). MS (ESI$^+$) m/z (%) = 1391.0 (14) $[M + PF_6 + 3H]^{2+}$, 1318.1 (15) $[M + 2H]^{2+}$, 1245.1 (19) $[M - PF_6 + H]^{2+}$, 1172.1 (31) $[M - 2PF_6]^{2+}$, 879.0 (78) $[M + 3H]^{3+}$, 830.4 (100) $[M - PF_6 + 2H]^{3+}$, 781.7 (83) $[M - 2PF_6 + H]^{3+}$, 763.0 (73) $[M - 2PF_6\text{-}C_4H_8 + H]^{3+}$, 744.4 (87) $[M - 2PF_6\text{-}2C_4H_8 + H]^{3+}$, 725.7 (70) $[M - 2PF_6 - 3C_4H_8 + H]^{3+}$, 707.0 (49) $[M - 2PF_6\text{-}4C_4H_8 + H]^{3+}$, 688.3 (33) $[M - 2PF_6\text{-}5C_4H_8 + H]^{3+}$, 669.6 (19) $[M - 2PF_6\text{-}6C_4H_8 + H]^{3+}$, 650.9 (14) $[M - 2PF_6\text{-}7C_4H_8 + H]^{3+}$, 632.2 (7) $[M - 2PF_6\text{-}8C_4H_8 + H]^{3+}$, 613.5 (4) $[M - 2PF_6\text{-}9C_4H_8 + H]^{3+}$, 595.0 (3) $[M - 2PF_6\text{-}10C_4H_8 + H]^{3+}$. HRMS (ESI$^+$) calcd for $C_{123}H_{171}N_{15}O_{24}Ru$ $[M - 2PF_6]^{2+}$, m/z 1172.0850; found, m/z 1172.0887. Calcd for $C_{123}H_{172}N_{15}O_{24}Ru$ $[M - 2PF_6 + H]^{3+}$, m/z 781.7260; found, m/z 781.7283. Anal. Calcd for $C_{123}H_{171}F_{12}N_{15}O_{24}P_2Ru$: C, 56.07; H, 6.54; N, 7.97. Found: C, 55.79; H, 6.65; N, 7.83.

Synthesis of Ruthenium(II) Complex [10] $(CF_3COO)_2$. To a stirring solution of **9** (53 mg, 20.1 μmol) in CH_2Cl_2 (6 mL) was added TFA (1.4 mL, 18.1 mmol) at 0 °C. The mixture was then stirred 24 h at room temperature. The solvent was coevaporated several times in vacuo with CH_3CN to give **10** as a red powder (38 mg, 100%). HPLC (system B): t_R = 3.9 min. ^{1}H NMR (300 MHz, D_2O) δ 8.72−8.58 (m, 6H), 8.37−8.30 (m, 3H), 8.12−7.79 (m, 9H), 7.51−7.35 (m, 9H), 4.85−4.59 (m, partially masked by H_2O signal), 4.14−3.97 (m, 24H). ^{13}C NMR (125 MHz, D_2O) δ 169.7−169.3 (3 signals, Cq), 163.1 and 162.8 (Cq), 157.9−157.7 (4 signals, Cq), 156.3 and 156.2 (Cq), 152.0−151.7 (3 signals, CH), 151.0−150.7 (4 signals, Cq), 149.7−149.1 (3 signals, CH), 146.2−146.0 (4 signals, Cq), 138.3−138.0 (3 signals, CH), 136.9 and 136.8 (CH), 136.0−135.9 (3 signals, Cq), 127.9 and 127.7 (CH), 125.0−124.9 (3 signals, CH), 123.5−123.1 (4 signals, CH), 119.8, 117.4, 115.1, and 112.8 (CF_3), 58.6−58.4 (4 signals, CH_2), 56.3 and 56.2 (CH_2). ^{19}F NMR (300 MHz, D_2O) δ −75.6 (CF_3). HRMS (ESI$^+$) calcd for $C_{75}H_{75}N_{15}O_{24}Ru$ $[M - 2CF_3COO]^{2+}$, m/z 835.7087; found, m/z = 835.7102. UV−vis (50 mM Tris buffer, pH 7.4): λ_{max}/nm (ε/M^{-1} cm^{-1}) = 299 (73 100), 468 (7100).

Synthesis of Lanthanide(III)−Ruthenium(II) Complexes. To a solution of complex **10** (78 mg, 41 μmol) in H_2O (7 mL) was added $LnCl_3{\cdot}6H_2O$ (139 μmol). After stirring at room temperature for 1 h, pH was adjusted to 5−6 with NaOH 0.1 M, and the mixture was then stirred 18 h at room temperature. The solvent was evaporated to a minimum, and the solution was loaded on a Waters Sep-Pak column (C_{18}, 10 g). The column was rinsed with 5 × 8 mL of H_2O to remove salts, and the product was eluted with a H_2O/MeOH mixture (1:1, 5 × 1 mL). The absence of free lanthanide ions was checked by the Arsenazo test. Yields were quantitative.

Gd_3Ru complex **1**: HPLC analysis (system C): t_R = 5.9 min. Anal. Calcd for $C_{75}H_{63}Gd_3N_{15}NaO_{24}Ru{\cdot}10H_2O$: C, 38.59; H, 3.58; N, 9.00. Found: C, 38.10; H, 3.49; N, 8.74. HRMS (ESI$^-$) calcd for $C_{75}H_{63}Gd_3N_{15}O_{24}Ru$ $[M - Na]^{2-}$, m/z 1065.5482; found, m/z 1065.5452. The ratio Gd/Ru determined by ICP-MS technique was 2.95:1.00.

Eu_3Ru complex **2**: HPLC analysis (system C): t_R = 6.0 min. HRMS (ESI$^+$) calcd for $C_{75}H_{66}Eu_3N_{15}O_{24}Ru$ $[M - Na + 3H]^{2+}$, m/z 1059.5548; found, m/z 1059.5511. HRMS (ESI$^-$) calcd for $C_{75}H_{63}Eu_3N_{15}O_{24}Ru$ $[M - Na]^{2-}$, m/z 1058.5470; found, m/z 1058.5448. Luminescence: λ_{em} (50 mM Tris buffer, pH 7.4, λ_{exc} = 299 nm, t_d = 50 μs)/nm 580 (relative intensity, corrected spectrum 2), 593 (28), 616 (100), 686, 699 (59).

Nd_3Ru complex **3**. HPLC analysis (system C): t_R = 6.0 min. MS (ESI$^-$) m/z 2091.1 $[M - Na]^-$.

Yb_3Ru complex **4**. HPLC analysis (system C): t_R = 5.8 min. MS (ESI$^-$) m/z 2178.2 $[M - Na]^-$.

■ ASSOCIATED CONTENT

Supporting Information

^{1}H and ^{13}C NMR spectra of compound **8** (Figure S1) and Ru(II) complex **9** (Figure S2); ^{13}C NMR spectrum of Ru(II) complex **10** (Figure S3); HPLC chromatogram of Gd_3Ru complex **1** (Figure S4); HRMS of Eu_3Ru complex **2** (Figure S5); R_1^P relaxivity as a function of the concentration in complex **1** (Figure S6); excitation and emission spectra of Ru(II) complex **10** (Figure S7); excitation spectrum of Eu_3Ru complex

DOI: 10.1021/ic502342x
Inorg. Chem. 2015, 54, 1414−1425

2 (Figure S8); evolution of the fluorescence spectrum of Ru(II) complex **10** upon addition of $YbCl_3$ solutions (Figure S9). This material is available free of charge via the Internet at http://pubs.acs.org.

AUTHOR INFORMATION

Corresponding Authors

*(L.V.E.) E-mail: luce.vanderelst@umons.ac.be.
*(B.M.-V.) E-mail: mestre@chimie.ups-tlse.fr.
*(C.P.) E-mail: picard@chimie.ups-tlse.fr.

Present Address

#(C.D.) CNRS, Laboratoire de Chimie de coordination (LCC), UPR 8241, 205 route de Narbonne, 31077 Toulouse cedex 4, France.

Author Contributions

A.B. and C.D. contributed equally to this work and should be considered as first authors.

Notes

The authors declare no competing financial interest.

ACKNOWLEDGMENTS

The authors thank Dr. Stéphane Balayssac and Prof. Alain Vigroux for fruitful discussions. This work was supported by the French Ministère de la Recherche (Ph.D. grant for A.B.) and the CNRS. The ARC (research contract AUWB-2010-10/15-UMONS-5), the FNRS, the Walloon Region, the COST TD1004 (Theranostics imaging and therapy: an action to develop novel nanosized systems for imaging-guided drug delivery), the UIAP VII program, the European Network of Excellence EMIL (European Molecular Imaging Laboratories) program LSCH-2004-503569, and the Center for Microscopy and Molecular Imaging (CMMI, supported by the European Regional Development Fund and the Walloon Region) are thanked for their support.

REFERENCES

(1) Heffern, M. C.; Matosziuk, L. M.; Meade, T. J. *Chem. Rev.* **2014**, *114*, 4496−4539.
(2) Caravan, P.; Zhang, Z. *Eur. J. Inorg. Chem.* **2012**, 1916−1923.
(3) Yang, C.-T.; Chuang, K.-H. *Med. Chem. Commun.* **2012**, *3*, 552−565.
(4) Helm, L. *Future Med. Chem.* **2010**, *2*, 385−396.
(5) Ni, Y.; Wang, H.; Chen, F.; Li, J.; DeKeyzer, F.; Feng, Y.; Yu, J.; Bosmans, H.; Marchal, G. *Methods* **2009**, *48*, 125−138.
(6) Laurent, S.; Vander Elst, L.; Muller, R. N. *Contrast Media Mol. Imaging* **2006**, *1*, 128−137.
(7) Caravan, P. *Chem. Soc. Rev.* **2006**, *35*, 512−523.
(8) Hermann, P.; Kotek, J.; Kubicek, V.; Lukes, I. *Dalton Trans.* **2008**, 3027−3047.
(9) Bryson, J. M.; Reineke, J. W.; Reineke, T. M. *Macromolecules* **2012**, *45*, 8939−8952.
(10) Villaraza, A. J. L.; Bumb, A.; Brechbiel, M. W. *Chem. Rev.* **2010**, *110*, 2921−2959.
(11) Botta, M.; Tei, L. *Eur. J. Inorg. Chem.* **2012**, 1945−1960.
(12) Jebasingh, B.; Alexander, V. *Inorg. Chem.* **2005**, *44*, 9434−9443.
(13) Livramento, J. B.; Helm, L.; Sour, A.; O'Neil, C.; Merbach, A. E.; Toth, E. *Dalton Trans.* **2008**, 1195−1202.
(14) Harrison, V. S. R.; Carney, C. E.; Macrenaris, K. W.; Meade, T. J. *Chem. Commun.* **2014**, *50*, 11469−11471.
(15) Comblin, V.; Gilsoul, D.; Hermann, M.; Humblet, V.; Jacques, V.; Mesbahi, M.; Sauvage, C.; Desreux, J. F. *Coord. Chem. Rev.* **1999**, *185−186*, 451−470.
(16) Costa, J.; Ruloff, R.; Burai, L.; Helm, L.; Merbach, A. E. *J. Am. Chem. Soc.* **2005**, *127*, 5147−5157.
(17) Paris, J.; Gameiro, C.; Humblet, V.; Mohapatra, P. K.; Jacques, V.; Desreux, J. F. *Inorg. Chem.* **2006**, *45*, 5092−5102.
(18) Livramento, J. B.; Sour, A.; Borel, A.; Merbach, A. E.; Toth, E. *Chem.—Eur. J.* **2006**, *12*, 989−1003.
(19) Moriggi, L.; Aebischer, A.; Cannizzo, C.; Sour, A.; Borel, A.; Bunzli, J.-C. G.; Helm, L. *Dalton Trans.* **2009**, 2088−2095.
(20) Li, W.-S.; Luo, J.; Chen, Z.-N. *Inorg. Chem. Commun.* **2011**, *14*, 1898−1900.
(21) Verwilst, P.; Eliseeva, S. V.; Vander Elst, L.; Burtea, C.; Laurent, S.; Petoud, S.; Muller, R. N.; Parac-Vogt, T. N.; De Borggraeve, W. M. *Inorg. Chem.* **2012**, *51*, 6405−6411.
(22) Dehaen, G.; Eliseeva, S. V.; Verwilst, P.; Laurent, S.; Vander Elst, L.; Muller, R. N.; De Borggraeve, W.; Binnemans, K.; Parac-Vogt, T. N. *Inorg. Chem.* **2012**, *51*, 8775−8783.
(23) Li, W.-S.; Luo, J.; Jiang, F.; Chen, Z.-N. *Dalton Trans.* **2012**, *41*, 9405−9410.
(24) Debroye, E.; Dehaen, G.; Eliseeva, S. V.; Laurent, S.; Vander Elst, L.; Muller, R. N.; Binnemans, K.; Parac-Vogt, T. N. *Dalton Trans.* **2012**, *41*, 10549−10556.
(25) Dehaen, G.; Eliseeva, S. V.; Kimpe, K.; Laurent, S.; Vander Elst, L.; Muller, R. N.; Dehaen, W.; Binnemans, K.; Parac-Vogt, T. N. *Chem.—Eur. J.* **2012**, *18*, 293−302.
(26) Debroye, E.; Parac-Vogt, T. N. *Chem. Soc. Rev.* **2014**, *43*, 8178−8192.
(27) Sung, S.; Holmes, H.; Wainwright, L.; Toscani, A.; Stasiuk, G. J.; White, A. J. P.; Bell, J. D.; Wilton-Ely, J. D. E. T. *Inorg. Chem.* **2014**, *53*, 1989−2005.
(28) Livramento, J. B.; Weidensteiner, C.; Prata, M. I. M.; Allegrini, P. R.; Geraldes, C. F. G. C.; Helm, L.; Kneuer, R.; Merbach, A. E.; Santos, A. C.; Schmidt, P.; Toth, E. *Contrast Media Mol. Imaging* **2006**, *1*, 30−39.
(29) Parac-Vogt, T. N.; Vander Elst, L.; Kimpe, K.; Laurent, S.; Burtéa, C.; Chen, F.; Van Deun, R.; Ni, Y.; Muller, R. N.; Binnemans, K. *Contrast Media Mol. Imaging* **2006**, *1*, 267−278.
(30) Jennings, L. E.; Long, N. J. *Chem. Commun.* **2009**, 3511−3524.
(31) Louie, A. *Chem. Rev.* **2010**, *110*, 3146−3195.
(32) Rivas, C.; Stasiuk, G. J.; Gallo, J.; Minuzzi, F.; Rutter, G. A.; Long, N. J. *Inorg. Chem.* **2013**, *52*, 14284−14293.
(33) Stasiuk, G. J.; Tamang, S.; Imbert, D.; Gateau, C.; Reiss, P.; Fries, P.; Mazzanti, M. *Dalton Trans.* **2013**, *42*, 8197−8200.
(34) Laus, S.; Sour, A.; Ruloff, R.; Toth, E.; Merbach, A. E. *Chem.—Eur. J.* **2005**, *11*, 3064−3076.
(35) Laurent, S.; Vander Elst, L.; Wautier, M.; Galaup, C.; Muller, R. N.; Picard, C. *Bioorg. Med. Chem. Lett.* **2007**, *17*, 6230−6233.
(36) Laurent, S.; Vander Elst, L.; Galaup, C.; Leygue, N.; Boutry, S.; Picard, C.; Muller, R. N. *Contrast Media Mol. Imaging* **2014**, *9*, 300−312.
(37) Dickins, R. S.; Aime, S.; Batsanov, A. S.; Beeby, A.; Botta, M.; Bruce, J. I.; Howard, J. A. K.; Love, C. S.; Parker, D.; Peacock, R. D.; Puschmann, H. *J. Am. Chem. Soc.* **2002**, *124*, 12697−12705.
(38) Pellegatti, L.; Zhang, J.; Drahos, B.; Villette, S.; Suzenet, F.; Guillaumet, G.; Petoud, S.; Toth, E. *Chem. Commun.* **2008**, 6591−6593.
(39) Caravan, P.; Ellison, J. J.; McMurry, T. J.; Lauffer, R. B. *Chem. Rev.* **1999**, *99*, 2293−2352.
(40) Moriggi, L.; Cannizzo, C.; Prestinari, C.; Berrière, F.; Helm, L. *Inorg. Chem.* **2008**, *47*, 8357−8366.
(41) Zhao, Q.; Huang, C.; Li, F. *Chem. Soc. Rev.* **2011**, *40*, 2508−2524.
(42) Fernandez-Moreira, V.; Thorp-Greenwood, F. L.; Coogan, M. P. *Chem. Commun.* **2010**, *46*, 186−202.
(43) Nonat, A. M.; Allain, C.; Faulkner, S.; Gunnlaugsson, T. *Inorg. Chem.* **2010**, *49*, 8449−8456.
(44) Nonat, A. M.; Quinn, S. J.; Gunnlaugsson, T. *Inorg. Chem.* **2009**, *48*, 4646−4648.
(45) Perry, W. S.; Pope, S. J. A.; Allain, C.; Coe, B. J.; Kenwright, A. M.; Faulkner, S. *Dalton Trans.* **2010**, *39*, 10974−10983.
(46) Schwab, P. F. H.; Fleischer, F.; Michl, J. *J. Org. Chem.* **2002**, *67*, 443−449.

DOI: 10.1021/ic502342x
Inorg. Chem. 2015, 54, 1414−1425

(47) Benaglia, M.; Toyota, S.; Woods, C. R.; Siegel, J. S. *Tetrahedron Lett.* **1997**, *38*, 4737−4740.
(48) Takalo, H.; Mukkala, V.-M.; Mikola, H.; Liitti, P.; Hemmila, I. *Bioconjugate Chem.* **1994**, *5*, 278−282.
(49) Metherell, A. J.; Cullen, W.; Stephenson, A.; Hunter, C. A.; Ward, M. D. *Dalton Trans.* **2014**, *43*, 71−84.
(50) Armstrong, E. A. P.; Brown, R. T.; Sekwale, M. S.; Fletcher, N. C.; Gong, X.-Q.; Hu, P. *Inorg. Chem.* **2004**, *43*, 1714−1722.
(51) Fletcher, N. C.; Nieuwenhuyzen, M.; Rainey, S. *J. Chem. Soc., Dalton Trans.* **2001**, 2641−2648.
(52) Hayes, M. A.; Meckel, C.; Schatz, E.; Ward, M. D. *J. Chem. Soc., Dalton Trans.* **1992**, 703−708.
(53) Josan, J. S.; De Silva, C. R.; Yoo, B.; Lynch, R. M.; Pagel, M. D.; Vagner, J.; Hruby, V. J. *Methods Mol. Biol.* **2011**, *716*, 89−126.
(54) Baranyai, Z.; Tei, L.; Giovenzana, G. B.; Kalman, F. K.; Botta, M. *Inorg. Chem.* **2012**, *51*, 2597−2607 and references therein.
(55) Nonat, A. M.; Gateau, C.; Fries, P. H.; Helm, L.; Mazzanti, M. *Eur. J. Inorg. Chem.* **2012**, 2049−2061.
(56) Livramento, J. B.; Toth, E.; Sour, A.; Borel, A.; Merbach, A. E.; Ruloff, R. *Angew. Chem. Int. Ed* **2005**, *44*, 1480−1484.
(57) Kotkova, Z.; Kotek, J.; Jirak, D.; Jendelova, P.; Herynek, V.; Berkova, Z.; Hermann, P.; Lukes, I. *Chem.—Eur. J.* **2010**, *16*, 10094−10102.
(58) Vander Elst, L.; Maton, F.; Laurent, S.; Seghi, F.; Chapelle, F.; Muller, R. N. *Magn. Reson. Med.* **1997**, *38*, 604−614.
(59) Muller, R.; Raduchel, B.; Laurent, S.; Platzek, J.; Pierart, C.; Mareski, P.; Vander Elst, L. *Eur. J. Inorg. Chem.* **1999**, 1949−1955.
(60) Micskei, K.; Helm, L.; Brucher, E.; Merbach, A. E. *Inorg. Chem.* **1993**, *32*, 3844−3850.
(61) Bonnet, C. S.; Buron, F.; Caillé, F.; Shade, C. M.; Drahos, B.; Pellegatti, L.; Zhang, J.; Villette, S.; Helm, L.; Pichon, C.; Suzenet, F.; Petoud, S.; Toth, E. *Chem.—Eur. J.* **2012**, *18*, 1419−1431.
(62) Caillé, F.; Bonnet, C. S.; Buron, F.; Villette, S.; Helm, L.; Petoud, S.; Suzenet, F.; Toth, E. *Inorg. Chem.* **2012**, *51*, 2522−2532.
(63) de Kemp, R. A.; Epstein, F. H.; Catana, C.; Tsui, B. M. W.; Ritman, E. L. *J. Nucl. Med.* **2010**, *51*, 18S−32S.
(64) Laurent, S.; Henoumont, C.; Vander Elst, L.; Muller, R. N. *Eur. J. Inorg. Chem.* **2012**, 1889−1915.
(65) Laurent, S.; Parac-Vogt, T. N.; Kimpe, K.; Thirifays, C.; Binnemans, K.; Muller, R. N.; Vander Elst, L. *Eur. J. Inorg. Chem.* **2007**, 2061−2067.
(66) Juris, A.; Balzani, V.; Barigelletti, F.; Campagna, S.; Belser, P.; Von Zelewsky, A. *Coord. Chem. Rev.* **1988**, *84*, 85−277.
(67) Kalyanasundaram, K. *Coord. Chem. Rev.* **1982**, *46*, 159−244.
(68) Lo, K. K.-W.; Lee, T. K.-M.; Lau, J. S.-Y.; Poon, W.-L.; Cheng, S.-H. *Inorg. Chem.* **2008**, *47*, 200−208 and references therein.
(69) Ishida, H.; Tobita, S.; Hasegawa, Y.; Katoh, R.; Nozaki, K. *Coord. Chem. Rev.* **2010**, *254*, 2449−2458.
(70) Supkowski, R. M.; Horrocks, W. D. W., Jr. *Inorg. Chim. Acta* **2002**, *340*, 44−48.
(71) Muller, R. N.; Declercq, D.; Vallet, P.; Giberto, F.; Daminet, B.; Fisher, H. W.; Maton, F.; Van Haverbeke, Y. In *Proceedings of the ESMRMB, 7th Annual Congress*, May 2−5, Strasbourg, France, 1990; p 394.
(72) Vallet P. *Relaxivity of Nitroxide Stable Free Radicals. Evaluation by Field Cycling Method and Optimisation*. Ph.D. Thesis, University of Mons, Belgium, 1992.
(73) Sun, Y.; Machala, M. L.; Castellano, F. N. *Inorg. Chim. Acta* **2010**, *363*, 283−287.

DOI: 10.1021/ic502342x
Inorg. Chem. 2015, 54, 1414−1425